3

Magnetic Force Microscopy:
Basic Principles and Applications

F.A. Ferri[1], M.A. Pereira-da-Silva[1,2] and E. Marega Jr.[1]
[1]Instituto de Física de São Carlos, Universidade de São Paulo, São Carlos
[2]Centro Universitário Central Paulista, UNICEP, São Carlos
Brazil

1. Introduction

Magnetic force microscopy (MFM) is a special mode of operation of the atomic force microscope (AFM). The technique employs a magnetic probe, which is brought close to a sample and interacts with the magnetic stray fields near the surface. The strength of the local magnetostatic interaction determines the vertical motion of the tip as it scans across the sample.

MFM was introduced shortly after the invention of the AFM (Martin & Wickramasinghe, 1987), and became popular as a technique that offers high imaging resolution without the need for special sample preparation or environmental conditions. Since the early 1990s, it has been widely used in the fundamental research of magnetic materials, as well as the development of magnetic recording components. MFM detects the quantity that is of particular interest for the magnetic recording process, namely the magnetic stray field produced by a magnetized medium or by a write head. The magnetic transition geometry and stray field configuration in longitudinal recording media is illustrated in Fig. 1 (Rugar et al., 1990). Nowadays, the main developments in MFM are focused on the quantitative analysis of data, improvement of resolution, and the application of external fields during measurements (Schwarz & Wiesendanger, 2008).

The interpretation of images acquired by MFM requires knowledge about the specific near-field magnetostatic interaction between probe and sample. Therefore, this subject will be briefly discussed hereafter. Other topics to be considered are the properties of suitable probes, the achievable spatial resolution, and the inherent restrictions of the method. More detailed information can be found, e.g., in articles by Rugar et al., Porthun et al. and Hartmann. Valuable information can also be found in the works of Koch and Hendrych et al.

In the present chapter, we will also demonstrate some applications of the technique made by our research group in the study of magnetic vortices formation in sub-microsized structures, as well as further magnetic properties, of Si and Ge-based magnetic semiconductors thin films.

2. Basics of magnetic contrast formation

The operating principle of MFM is the same as in AFM. Both static and dynamic detection modes can be applied, but mainly the dynamic mode is considered here because it offers
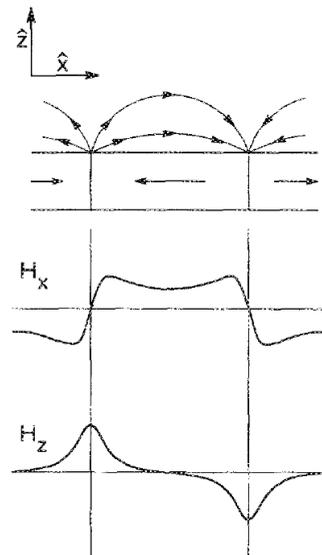
Fig. 1. Geometry of the magnetic stray field above a longitudinal magnetic medium (upper). Typical variation of the H_x and H_z components above the medium (lower) (Rugar et al., 1990)

better sensitivity. The cantilever (incorporating the tip) is excited to vibrate close to its resonance frequency, with a certain amplitude and a phase shift with respect to the drive signal. The deflection sensor of the microscope monitors the motion of the tip. Under the influence of a probe-sample interaction, the cantilever behaves as if it had a modified spring constant, $c_F = c - \partial F / \partial z$, where c is the natural spring constant and $\partial F / \partial z$ is the derivative of the interaction force relative to the perpendicular coordinate z. It is assumed that the cantilever is oriented parallel to the sample surface.

An attractive interaction with $\partial F / \partial z > 0$ will effectively make the cantilever spring softer, so that its resonance frequency will decrease. A shift in resonance frequency will lead to a change of the oscillation amplitude of the probe and of its phase. All of these are measurable quantities that can be used to map the lateral variation of $\partial F / \partial z$. The most common detection method uses the amplitude signal and is referred to as amplitude modulation (AM). The cantilever is driven slightly away from resonance, where the slope of the amplitude-versus-frequency curve is high, in order to maximize the signal obtained from a given force derivative.

Measurement sensitivity, or the minimum detectable force derivative, has an inverse dependence on the Q value of the oscillating system (Hartmann, 1999). Therefore, a high Q value might seem advantageous, but this has the drawback that it increases the response time of the detection system. In situations where Q is necessarily high, for example when scanning in vacuum, a suitable alternative is the frequency modulation (FM) technique (Porthun et al., 1998; Hartmann, 1999). In this method the cantilever oscillates directly at its resonance frequency by using a feedback amplifier with amplitude control.

The force derivative $\partial F / \partial z$ can originate from a wide range of sources, including electrostatic probe-sample interactions, van der Waals forces, damping, or capillary forces (Porthun et al., 1998). However, MFM relies on those forces that arise from a long-range magnetostatic coupling between probe and sample. This coupling depends on the internal magnetic structure of the probe, which greatly complicates the mechanism of contrast formation.

In general, a magnetized body, brought into the stray field of a sample, will have the magnetic potential energy E (Porthun et al., 1998):

$$E = -\mu_0 \int \vec{M}_{tip} \cdot \vec{H}_{sample} dV_{tip} \qquad (1)$$

where μ_0 is the vacuum permeability. The force acting on an MFM tip can thus be calculated by:

$$\vec{F} = -\vec{\nabla} E = \mu_0 \int \vec{\nabla} \left(\vec{M}_{tip} \cdot \vec{H}_{sample} \right) dV_{tip} \qquad (2)$$

The integration has to be carried out over the tip volume, or rather its magnetized part as illustrated in Fig. 2. Simplified models for the tip geometry and its magnetic structure are often used in order to make such calculations feasible. Another equivalent approach is to start the simulation with the tip stray field and to integrate over the sample volume (Porthun et al., 1998). According to Newton's third law, the force acting on the sample in the field of the tip is equal in magnitude to $\vec{F}$ in the previous equation:

$$\vec{F} = \mu_0 \int \vec{\nabla} \left(\vec{M}_{sample} \cdot \vec{H}_{tip} \right) dV_{sample} \qquad (3)$$
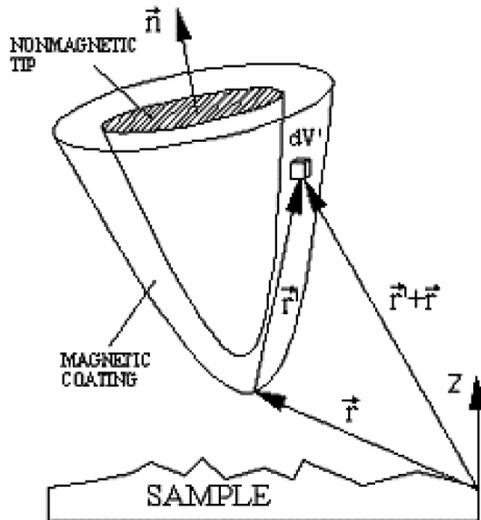

Fig. 2. Modelled MFM tip having a magnetic coating on a non-magnetic core. Parameters for integration are indicated (Koch, 2005)

The magnetostatic potential $\phi_s(\vec{r})$ created by any ferromagnetic sample can be calculated from its magnetization vector field $\vec{M}_s(\vec{r}')$ (Hartmann, 1999):

$$\phi_s(\vec{r}) = \frac{1}{4\pi}\left[\int \frac{d^2\vec{s}' \cdot \vec{M}_s(\vec{r}')}{|\vec{r}-\vec{r}'|} - \int d^3\vec{r}' \frac{\vec{\nabla} \cdot \vec{M}_s(\vec{r}')}{|\vec{r}-\vec{r}'|}\right] \tag{4}$$

where $\vec{s}'$ is an outward normal vector from the sample surface. The first (two-dimensional) integral covers all surface charges created by magnetization components perpendicular to the surface, while the second (three-dimensional) integral contains the volume magnetic charges resulting from interior divergences of the magnetization vector field. The sample stray field is then given by $\vec{H}_{sample}(\vec{r}) = -\vec{\nabla}\phi_s(\vec{r})$, which can be substituted in Equation (2) to calculate the interaction force $\vec{F}$. In static mode the instrument detects the vertical component of the cantilever deflection, $F_d = \vec{n} \cdot \vec{F}$, where $\vec{n}$ is an outward unit normal from the cantilever surface. In the dynamic mode the compliance component or force derivative $F_{d'}(\vec{r}) = (\vec{n} \cdot \vec{\nabla})[\vec{n} \cdot \vec{F}(\vec{r})]$ is detected (Hartmann, 1999).

A limitation in the use of MFM is that the magnetic configuration of the sensing probe is rarely known in detail. Although the general theory of contrast formation still holds, it is not possible to model the measured signal from first principles for an unknown domain structure of the magnetic probe. As a consequence, MFM can generally not be performed in a quantitative way, in the sense that a stray field would be detected in absolute units. Furthermore, because MFM is sensitive to the strength and polarity of near-surface stray fields produced by ferromagnetic samples, rather than to the magnetization itself, it is usually not straightforward to deduce the overall domain topology from an MFM image. The problem of reconstructing a concrete arrangement of inner and surface magnetic charges from the stray fields they produce is not solvable. MFM can, however, be used to compare the experimentally detected stray field variation of a micromagnetic object to that obtained from certain model calculations. This often enables to at least classify the magnetic object under investigation (Hartmann, 1999). Thus, even without detailed quantitative analysis, the qualitative information collected by the microscope can be very useful (Rugar et al., 1990).

3. Modelling the MFM response

If one wants to analyze the force derivative $F_{d'}(\vec{r})$ using Equations (2) and (4), then a model of the tip shape and magnetization must be constructed. Various levels of complexity are possible. Most models assume that both the tip and the sample are ideally hard magnetic materials, with a magnetization that is unaffected by the stray field from the other.

The simplest way to model a tip is with the point-probe approximation (Hartmann, 1999). The effective monopole and dipole moments of the probe are projected into a fictitious probe of infinitesimal size that is located a certain distance away from the sample surface. The unknown magnetic moments as well as the effective probe-sample separation are treated as free parameters to be fitted to experimental data. The force acting on the probe, which is immersed in the near-surface sample microfield, is given by (Hartmann, 1999):

$$\vec{F} = \mu_0\left(q + \vec{m} \cdot \vec{\nabla}\right)\vec{H} \tag{5}$$

where q and $\vec{m}$ are the effective monopole and dipole moments of the probe.

The point-probe approximation yields satisfactory results in many cases of MFM contrast interpretation. However, a far more realistic approach can be achieved by considering the extended geometry of a probe. An example is the pseudodomain model (Hartmann, 1999), in which the unknown magnetization vector field near the probe apex, with its entire surface and volume charges, is modelled by a homogeneously magnetized prolate spheroid of suitable dimensions. The magnetic response of the probe outside this imaginary domain is neglected. This pseudodomain model allows interpretation of most results obtained by MFM on the basis of bulk probes. For probes with a different geometry, for example those where the magnetic region is confined to a thin layer, other appropriate models have been developed (Rasa et al., 2002).

Fig. 3 shows both the measured and calculated MFM response across a series of 5 µm longitudinal bits (Rugar et al., 1990). The signal was recorded as a constant force derivative contour. In this particular case, the tip was modelled as a uniformly magnetized truncated cone with a spherical cap, in agreement with the shape as observed by electron microscopy (Rugar et al., 1990). Note that for in-plane magnetized samples, interdomain boundaries are the only sources of magnetic stray field that can be externally detected by MFM. On the other hand, samples with perpendicular magnetic anisotropy produce extended surface charges that correspond to the upward and downward pointing domain magnetization. In this case the near-surface stray field is directly related to the domain topology (Hartmann, 1999).
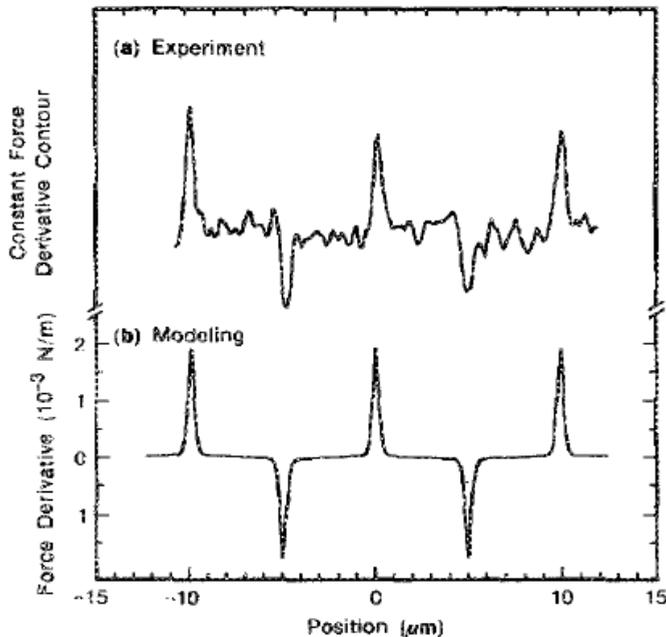

Fig. 3. (a) Contour of constant force derivative measured on a 5 µm bit sample. (b) Corresponding model calculation of magnetic force derivative (adapted from Rugar et al., 1990)

Usually, the MFM response of a certain tip-sample configuration is calculated by an integration in the spatial domain, e.g., over the sample volume. Porthun et al. have proposed a different formalism, where the problem is approached in the frequency domain. This has the advantage that it shows some characteristics of the imaging process more clearly. To be specific, the sample magnetization distribution is split up into harmonics, each having a spatial wavelength λ and wavenumber $k = 2\pi / \lambda$. The wavelength measures the length scale over which the magnetization vector goes through a complete rotation. Frequency components of the magnetic potential and the stray field are calculated separately. Then, the magnetic signal can be determined using Equation (2) for each of the stray field harmonics. For a specific (and simplified) tip-sample geometry (Fig. 4), the detected MFM signal is obtained by summing over all frequency components of the force derivative. The resulting signal, expressed in terms of sample magnetization and spatial frequency, forms a tip transfer function for the imaging process. An important observation is that the transfer function shows an exponential decay, $\exp(-kz_0)$, with increasing tip-sample distance z_0. It is thus crucial for high resolution to keep the tip-sample distance as small as possible. In addition, the dimensions (length, width, thickness) of a bar-type tip lead to specific decay rates both at high and low spatial frequencies. The latter illustrates that the finite size of a tip plays an important role in the imaging process. Therefore, a simple point-probe approximation is not sufficient to clarify how high and low spatial frequencies are attenuated. In the context of such a frequency domain description, the resolution can be defined as a minimum detectable wavelength which is determined by the noise limit of the detector system.
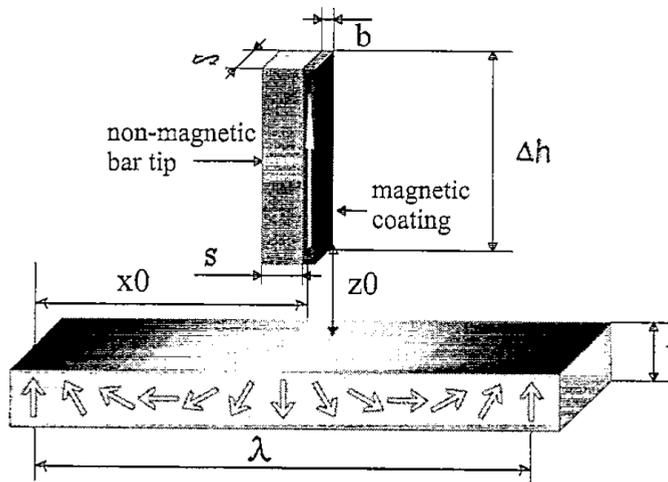

Fig. 4. One-dimensional model for the MFM measurement process (Porthun et al., 1998)

4. Requirements for MFM tips

The cantilever/tip assembly is obviously the critical element of a magnetic force microscope. Unlike in scanning tunnelling microscopy (STM) and repulsive-mode AFM, the tip shape is

important due to the long-range nature of magnetic forces (Rugar et al., 1990). Originally, electrochemically etched wires of cobalt or nickel were used as cantilevers (Martin & Wickramasinghe, 1987). Thanks to the widespread use of AFM, cantilevers with integrated sharp tips are now fabricated in large numbers out of silicon-based materials. These tips can be coated with a thin layer of magnetic material for the purpose of MFM observations. A lot of effort has been spent on the optimization of magnetic tips in order to get quantitative information from MFM data (Rugar et al., 1990; Porthun et al., 1998; Hartmann, 1999). The problem is that in the coating of conventional tips, a pattern of magnetic domains will arrange, which reduces the effective magnetic moment of the tip. The exact domain structure is unknown and can even change during MFM operation. Nevertheless, some information on the magnetization state of selected probes has been acquired using electron holography (Rugar et al., 1990; Hartmann, 1999).

The spatial resolution in MFM imaging is related to the tip-sample distance, but also to the magnetized part of the tip that is actually exposed to the sample stray field. Thus in order to improve lateral resolution, it is beneficial to restrict the magnetically sensitive region to the smallest possible size. Ideally the effective volume of the probe would consist of a small single-domain ferromagnetic particle located at the probe apex. So-called supertips have been developed based on this idea (Hartmann, 1999). However, there is a physical lower limit for the dimensions because an ultra-small particle becomes superparamagnetic.

The demand for a strong signal, produced by a small sensitive volume, indicates the need to maximize the magnetic moment in the tip. For this reason a single domain tip will give the best results and is also easier to describe theoretically. Materials with a high saturation magnetization should be used in order to limit the required volume. The well-defined magnetic state of a tip should be stable during scanning, and it should interfere as little as possible with the sample magnetization. A high switching field of the tip can be realized through the influence of shape anisotropy (Porthun et al., 1998; Hartmann, 1999), which forces the magnetization vector field near the probe apex to align with its axis of symmetry. Eventually, the smallest detail from which a sufficient signal-to-noise ratio can be gained is determined by the sensitivity of the deflection sensor, as well as the noise characteristics of the cantilever (Porthun et al., 1998).

In the present work, we have employed etched silicon tips of the MESP type supplied by Bruker. These are standard probes for MFM, and have a pyramidal geometry (Fig. 5). The magnetic coating consists of ~ 10–150 nm of Co/Cr alloy (exact thickness and composition of the coatings are undisclosed). The cantilever has a length L of approximately 225 μm. As a result, the resonance frequency f_0 is about 75 kHz. The coating has a coercivity of ~ 400 Oe and a magnetic moment of 1×10^{-13} emu. In order to ensure a predominant orientation of the magnetic vector field along the major probe axis, the thin film probes were magnetized (along the cantilever) prior to taking measurements. The Digital Instruments company offers a magnetizing device that possesses a permanent magnet. This apparatus ensures that the distance from the magnet to the tip is always the same in different magnetization procedures. Thus, taking into account that the magnetic field lines are dependent on the distance, the reproducibility is then guaranteed.
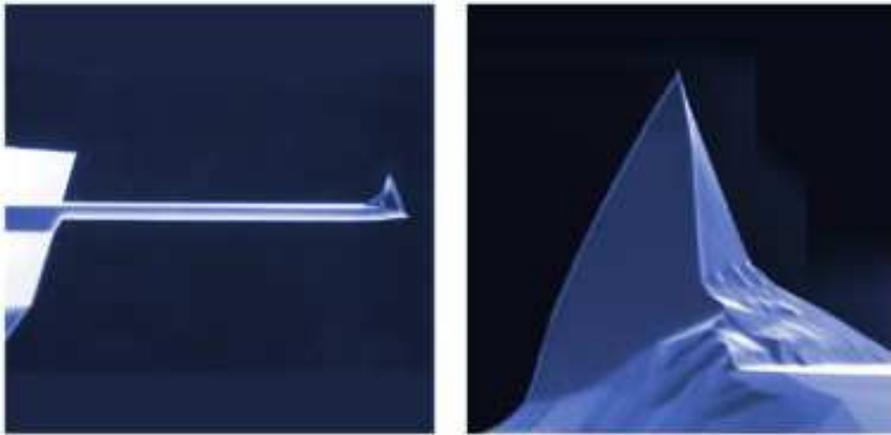
Fig. 5. Scanning electron images of AFM probes like the ones used for MFM. The probes are coated with a magnetic thin film. Specifications are mentioned in the text (Bruker Corporation, 2011)

5. Imaging procedure

As in AFM scanning, the detector signal can be fed back to the scanner z actuator. This mode of operation is called constant signal mode, in contrast to the open-loop or constant distance mode. The constant signal mode is robust and allows an accurate tracking of the sample surface, but it also presents a few problems. For example, the magnetic signal can be positive or negative, while stable feedback is only possible when the interaction does not change sign. This makes it necessary to bias the signal: the application of a voltage between the sample and the tip introduces an additional (electrostatic) force. Another problem of this mode is that the magnetic and non-magnetic interactions are mixed. The mixing ratio depends on the tip-sample distance which itself depends on the magnetic interaction. This makes the contributions very difficult to separate. For operation in air, it is known that the interaction with the surface contaminant layer and the damping (in dynamic mode) have a stronger influence on the tip than the van der Waals interaction (Porthun et al., 1998).

Quantitative data about the sample stray field can only be derived from MFM images when topographic signal contributions are not included. This is especially important when the tip is brought very close to the sample (in order to improve resolution), since non-magnetic forces become increasingly stronger. The solution to this problem is to keep the topography influence constant by letting the tip follow the surface height profile (Porthun et al., 1998). This constant distance mode places higher demands on instrument stability, because it is sensitive to drift. In the Digital Instruments microscope (Nanoscope 3A Multimode), the specific method employed to separate signal contributions is called lift mode (Fig. 6). It involves measuring the topography on each scan line in a first scan (left panel), and the magnetic information in a second scan of the same line (right panel). The difference in height Δh between the two scans, the so-called lift height, is selected by the user. Topography is measured in dynamic AM mode and the data is recorded to one

image. This height data is also used to move the tip at a constant local distance above the surface during the second (magnetic) scan line, during which the feedback is turned off. In theory, topographic contributions should be eliminated in the second image.
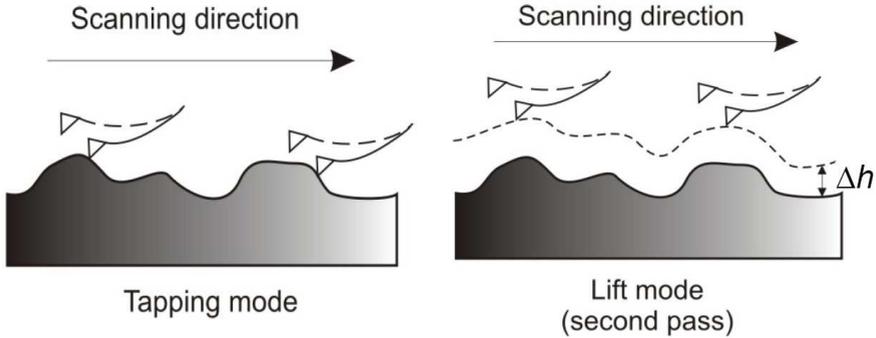

Fig. 6. Outline of the lift mode principle. Magnetic information is recorded during the second pass (right panel). The constant height difference between the two scan lines is the lift height Δh (adapted from Hendrych et al., 2007)

Magnetic data can be recorded either as variations in amplitude, frequency, or phase of the cantilever oscillation. It is argued that phase detection and frequency modulation give the best results, with a higher signal-to-noise ratio (Porthun et al., 1998; Hartmann, 1999). However, these detection modes can require the addition of an electronics module to the microscope. In our MFM measurements we have used amplitude detection, which measures changes in the cantilever's amplitude of oscillation relative to the piezo drive. The signal depends on the force derivative in the following manner (Porthun et al., 1998):

$$f = f_0 \sqrt{1 - \frac{\partial F / \partial z}{c}} \qquad (6)$$

with f_0 the free resonance frequency of the cantilever in the case of no tip sample interaction. In the amplitude detection, the cantilever is oscillated at a fixed frequency $f_{ext} > f_0$, where in the case of $\partial F / \partial z = 0$ the oscillation amplitude is already slightly below the maximum amplitude at f_0. When the resonance frequency changes this will result in a change in cantilever oscillation amplitude which can easily be detected. The disadvantage of this technique is that it is very slow for cantilevers with low damping and that a change in cantilever damping will be misinterpreted as change in resonance frequency.

It should be noted that an attractive interaction ($\partial F / \partial z > 0$) leads to a negative amplitude change (dark contrast in the image), while a repulsive interaction ($\partial F / \partial z < 0$) gives a positive amplitude variation (bright contrast).

Finally, Fig. 7(b) shows a typical MFM image. In this case, the sample was a piece of metal evaporated tape: a standard sample that is used to check whether the microscope is correctly tuned to image magnetic materials (Koch, 2005). It is clear that no correlation exists between the topography data shown on the left, and the magnetic data on the right. Consequently, the separation of both contributions is successful.
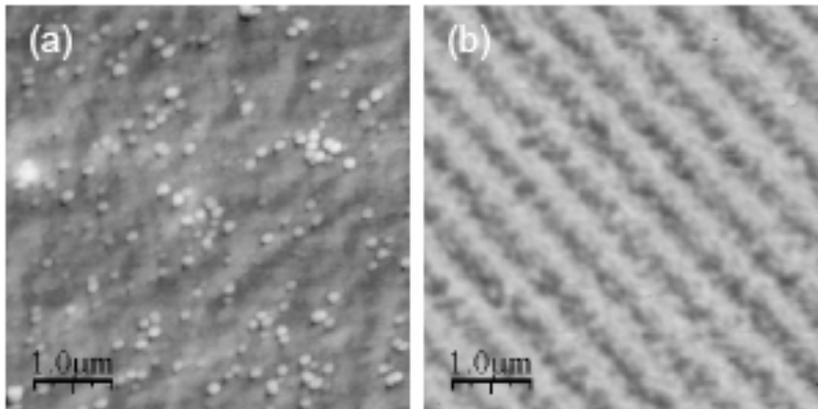
Fig. 7. Topographic image (a) and magnetic force gradient image (b) of a metal evaporated tape (Koch, 2005)

6. Applications of MFM in the study of Si and Ge-based magnetic semiconductors

6.1 Motivation

Driven by the promise of controlling charge and spin degrees of freedom, and its consequent technological impact through the realization of spintronic devices, many different ferromagnetic (FM) semiconductors have been investigated over the last few years. The potential advantages of this class of devices (in the form of ultra-dense non-volatile semiconductor memories, spin transistors and light emitting devices with polarized output, etc.) are expected to be, in addition to the low energy required to flip a spin: higher speed, greater efficiency and better stability (Zutic et al., 2004). Thus far, most of the work on FM semiconductors has been focused on Mn-containing II–VI or III–V compounds in which manganese replaces a fraction of group II or III sub-lattices (Dietl & Ohno, 2006). For practical reasons, however, the interest in a specific FM semiconductor depends on the existence of magnetic activity near or above room temperature as well as its compatibility with the current micro-electronics industry. Mn-containing Si- or Ge-based compounds partially fit these requirements since they possess a mature processing technology and because of some recent experimental work reporting Curie temperatures well above 300 K (Zhang et al., 2004; Kim et al., 2007). Furthermore, the low solubility of Mn in crystalline (c-)Si or c-Ge can be partially circumvented by using their amorphous counterparts, which also provide a more homogenous Mn distribution. Indeed, this is a particularly interesting feature since charge and spin states are sensitive mostly to the local environment so the magnetic activity existing in c-Si or c-Ge should also be observable in amorphous Si or Ge.

Based on these facts, this section reports on the MFM characterization of amorphous Si and Ge thin films containing different amounts of Mn and Co. Even though the amorphous character of the as-deposited films, thermal annealing at increasing temperatures induces their crystallization. Following this procedure, their magnetic properties have been systematically investigated as a function of the impurity concentration and atomic structure.

6.2 Experimental considerations

Thin films of amorphous SiMn and GeMn were prepared by conventional radio frequency sputtering. The Mn concentration ([Mn]) in the samples was in the ~ 0.1–24 at.% concentration range. Additionally, thin films of amorphous SiCo and GeCo were also deposited by sputtering. The Co concentration ([Co]) in the samples stayed in the ~ 1.7–10.3 at.% range. Pure samples were also prepared following identical conditions. The films, typically 1700 nm thick, were deposited principally on c-quartz and c-Si substrates. After deposition the films were submitted to thermal annealing treatments in the range of 200−900 ᵒC. The samples were characterized by a great variety of experimental techniques: (1) the composition of the films was determined mainly by energy dispersive x-ray spectrometry (EDS), (2) the atomic structure of the films was investigated by Raman scattering spectroscopy and x-ray diffraction (XRD) experiments, (3) the surface of the films was investigated by scanning electron microscopy (SEM) and AFM, (4) their optical properties were examined by means of transmission measurements, (5) the electrical resistivity of the films was measured using the standard van der Pauw technique, and (6) their magnetic properties were investigated by superconducting quantum interference device (SQUID) magnetometry and MFM. Except the SQUID measurements, all experimental characterizations were always carried out at room temperature. For further details, see Ferri et al., 2009a, 2009b, 2010a, 2010b, 2011.

6.3 Results and discussion

As confirmed by the Raman measurements, as the thermal annealing advances, the SiMn samples show crystallization signals that are accompanied by the growth of randomly dispersed sub-micrometre structures on the surface of the films. These structures are Mn-containing Si crystallites, surrounded by Si crystallites, amorphous Si and the $MnSi_{1.7}$ silicide phase (Ferri et al., 2009a). It is worth mentioning that the $MnSi_{1.7}$ is representative of a group of several Mn-silicides of the Mn_xSi_y form, with y/x approximately equal to 1.7: Mn_4Si_7, $Mn_{15}Si_{26}$, $Mn_{27}Si_{47}$, etc. Therefore, in this work, the Mn-silicides are simply identified by $MnSi_{1.7}$.

The morphology and magnetic characteristics of the $SiMn_{20\%}$ sample were investigated by means of AFM and MFM measurements (Fig. 8). Based on the AFM results the observed structures are typically ~ 750–1200 nm large and 300–400 nm high. Also, the image contrast present in Fig. 8(b) is a clear indication of the magnetic activity present in sample $SiMn_{20\%}$. At these dimensions, the contrast shown by the MFM images occurs because of force gradients between the FM tip and the magnetic activity present on the sample's surface. In this study, the MFM images were achieved after topography measurements (tapping mode) followed by sample surface scanning at a constant 200 nm height (lift mode). According to this procedure, no van der Waals forces are expected to be detected, and any change in the vibration amplitude of the cantilever is proportional to the gradient of magnetic fields perpendicular to the sample surface (Hartmann, 1999). It is worth noting that no MFM contrast was observed in the Mn-free film and $SiMn_{20\%}$ sample as-deposited nor after scanning the samples under the tapping mode.

In addition to the presence of magnetic activity in the sample under study, it also produces a remarkable contrast in the MFM image of Fig. 8(b). The FM materials are known to form
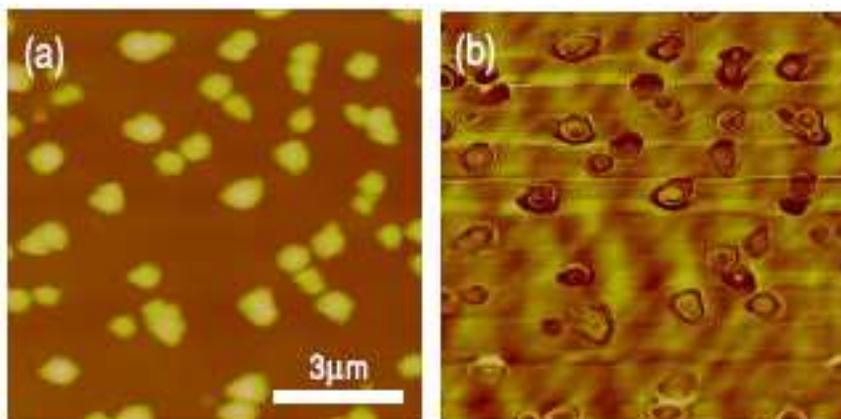
Fig. 8. (a) AFM and (b) MFM images of the sputter-deposited $SiMn_{20\%}$ film after thermal annealing at 600 ºC. The AFM scanning was performed in the tapping mode, whereas MFM in the lift mode by means of a Co/Cr coated tip magnetized just before scanning. The measurements were carried out under room conditions (temperature and atmosphere) from a 1.7 μm thick film deposited on crystalline silicon (Ferri et al., 2009a)

domain structures to reduce their magnetostatic energy that, at very small dimensions such those experienced by a (sub-)micrometre dot, for example, adopts the configuration of a curling spin or magnetization vortex (Shinjo et al., 2000). When the dot thickness becomes much smaller than the dot diameter, all spins tend to align in-plane. In the curling configuration, the spin directions change gradually in-plane in order to maintain the exchange energy and to cancel the total dipole energy (Fig. 9). The development of these magnetic vortices is well documented in the literature and its comprehensive description can be found in many works (Zhu et al., 2002; Soares et al., 2008).
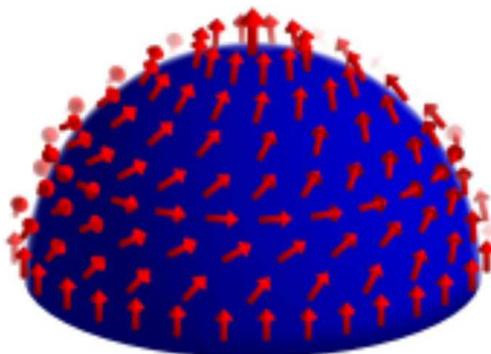

Fig. 9. Drawing of the magnetic moment configuration for ferromagnetic tri-dimensional sub-micrometre structures (Soares et al., 2008). At these very small dimensions, the magnetization adopts the pattern of a curling spin or magnetization vortex. In this curling arrangement, the spin directions change gradually in-plane in order to maintain the exchange energy and to cancel the total dipole energy

In this case, basically, the observed magnetic contrast occurs because of variations in the magnetization orientation along the sub-micrometre structures [Fig. 8(b)]. In other words, the presence of these Mn-based structures (probably Mn dimmers, in combination with the $MnSi_{1.7}$ phase) can lead to the appearance of magnetic activity (Bernardini et al., 2004; Affouda et al., 2006) whose main characteristics are highly influenced by the size and shape of the structures. Fig. 10 shows the surface topography in connection with the measured magnetic contrast of a single sub-micrometre structure. The figure also displays the height profile and MFM voltage achieved under horizontal [Fig. 10(b)], vertical [Fig. 10(c)] and diagonal [Fig. 10(d)] scans along the structure.
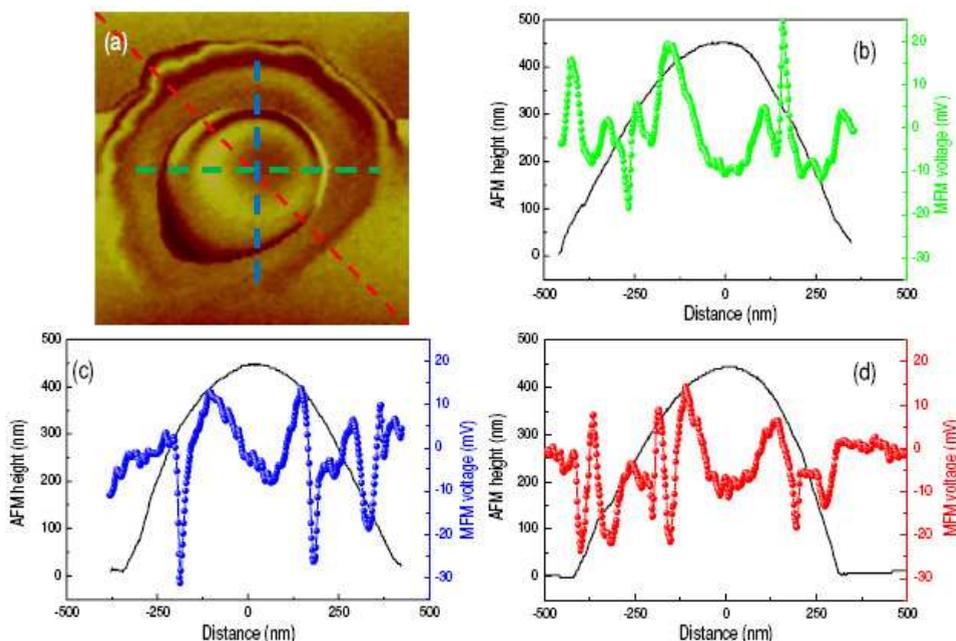

Fig. 10. (a) Magnetic force microscopy image of an isolated sub-micrometre structure present in the $SiMn_{20\%}$ film after thermal annealing at 600 °C. Its height profile (as obtained by AFM) and corresponding MFM voltage along the horizontal, vertical and diagonal dashed lines drawn in (a) are represented, respectively, in (b), (c) and (d). Note the MFM voltage pattern due to the presence of magnetic vortices in the structure (Ferri et al., 2009a)

It is interesting to observe the quite different topographic (AFM profile) and magnetic (MFM voltage) patterns achieved from the very same structure exclusively due to the presence of magnetic activity. The effect of manganese on the formation of these magnetic vortices is also remarkable suggesting that, once the structure is formed, the Mn distribution is non-uniform (and/or highly influenced by the presence of $MnSi_{1.7}$) around it.

The Mn-free, $GeMn_{3.7\%}$ and $GeMn_{24\%}$ films deposited under crystalline quartz substrates were also investigated through similar MFM measurements (Ferri et al., 2010a). Since these samples showed a flat surface, the magnetic activity of these three films was evaluated by scanning the MFM tip along a ~ 20 µm line across the crystalline quartz substrate partially

covered by the desired Ge film (see sketch in Fig. 11). By adopting this procedure, at the bare substrate-film edge, the MFM tip will experience a signal difference which is proportional to the magnetic response of the probed region. Considering that crystalline quartz gives no magnetic contrast in the MFM measurements, the observed MFM signal is exclusively due to the GeMn films. In fact, and in accord with the literature (Cho et al, 2002) and our SQUID results, no MFM signal has been observed from both the amorphous and crystallized Mn-free Ge films. Also, and in order to confirm that the MFM signal is mainly of magnetic nature (Porthun et al., 1998), the measurements were carried out at a fixed tip-to-sample (substrate + film) distance d in the $100-2500$ nm range. The main results of these MFM measurements, in conjunction with the SQUID data, are shown in Fig. 11. Here it is important to point out that similar results were obtained for the SiMn samples according this procedure (not shown).
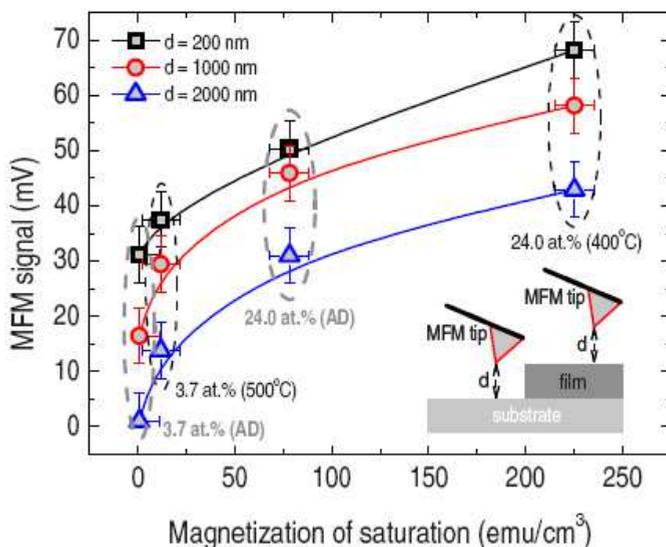

Fig. 11. MFM signal (as obtained from the voltage difference at the bare substrate-film edge region—see sketch) as a function of the magnetization of saturation (as obtained from the SQUID measurements at $T \geq 300$ K). The MFM data correspond to three different MFM tip-to-sample distances ($d = 200$, 1000, and 2000 nm). The measurements were carried out on the GeMn$_{3.7\%}$ and GeMn$_{24\%}$ films, deposited on crystalline quartz: both amorphous (AD—as-deposited) and after crystallization at the temperatures indicated in the figure. The lines joining the experimental data points are just guides to the eye (Ferri et al., 2010a)

The experimental data of Fig. 11 indicates that the MFM signal decreases with the distance d : demonstrating the magnetic character behind the interaction between the MFM tip and the sample. Except for minor deviations in the MFM signals obtained with the lowest d values, which were clearly affected by the experimental conditions (temperature, film thickness, and instrumental resolution, for example), the MFM signal scales with the magnetization of saturation, as obtained from the SQUID measurements. Indeed, the MFM signal increases with [Mn] and after the crystallization of the GeMn films. Therefore, as far

as absolute magnetic data are available (such as those given by SQUID magnetometry, for example) the adopted experimental procedure can provide a convenient method to analyze the magnetic properties of microsized (or sub-microsized) isolated systems. As a final point, it is important to mention that the room temperature magnetic activity observed in the present GeMn samples (Fig. 11), occurs, basically, because of the presence of the Mn_5Ge_3 ferromagnetic germanide phase (Ferri et al., 2009b, 2010a).

For the magnetic characterization of the SiCo and GeCo films (deposited on crystalline quartz) the MFM technique was used similarly to the GeMn samples, since these samples also showed a flat surface (Ferri et al., 2010b). The main results of these MFM measurements are shown in Fig. 12, which illustrates results obtained in some SiCo and GeCo samples without annealing and after thermal treatment up to the crystallization temperature. In these samples, after crystallization, the non-magnetic $CoSi_2$ silicide and $CoGe_2$ germanide phases were found, as confirmed by XRD measurements (not shown). Therefore, we must to keep in mind that the only phase that can cause ferromagnetism at room temperature (or higher) for the samples in question, is the metallic Co, which has a Curie temperature of ~ 1382 K (Ko et al., 2006).
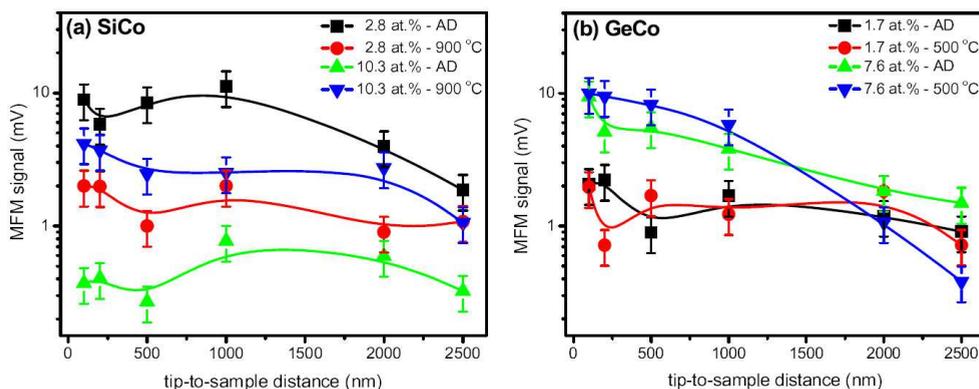

Fig. 12. MFM signal (as obtained from the voltage difference at the bare substrate-film edge region−see sketch of Fig. 11) as a function of the tip-to-sample distance, for as-deposited (AD) and thermally annealed (a) SiCo and (b) GeCo films (pure and containing different amounts of Co) deposited on c-quartz. The Co contents and the annealing temperatures are indicated in the figure. The lines joining the experimental data points are just guides to the eye

The MFM measurements for the Co-free Si and Ge films (both amorphous and annealed up to the crystallization temperature) suggest the absence of magnetic activity. This experimental result is expected [since it was also observed in the set of Mn-free Si and Ge samples (Ferri et al., 2009a, 2010)], and is in accord with the literature (Bolduc et al., 2005; Cho et al., 2002). When annealed at high temperatures, the XRD results indicate the presence of non-magnetic phases in the films containing Co. In addition, it is known that Co is less efficient than Mn in promoting ferromagnetic alignment, and a high magnetic moment, for the case of Ge (Continenza et al., 2006). Therefore, we expect a similar magnetic behaviour from the Co for the Si matrix. Taking these considerations into account, and remembering the fact that the MFM experiments were performed at room temperature, it is expected for

the present samples a very weak or at least less intense magnetic signal than in the case of the Mn-containing films. Therefore, the results of Fig. 12 are in agreement with the initial expectations. Unlike observed in samples with Mn it is possible to identify only a slight decrease in the MFM signal with the tip-sample separation, due to the comparatively lower signal intensity. Here it is important to notice that the present procedure adopted in the MFM measurements is unique in the literature. Consequently, similar results obtained from others, for quantitative comparison purposes, are non-existent.

For the GeCo samples, we observed that the MFM signal intensity increased with increasing Co concentration [see Fig 12(b)]. The thermal treatment for samples with the same [Co], in principle, didn't intensify the magnetic signal. As an example of increasing MFM signal intensity with [Co], at a tip-sample separation of 500 nm, we observed that the Ge film with [Co] ~ 1.7 at.% showed a MFM signal of ~ 2 mV , and the Ge film with [Co] ~ 7.6 at.% exhibited a MFM signal of ~ 8 mV, both annealed at 500 $^{\circ}$C. Still, as can be seen in Fig. 12(b), even the as-deposited Ge samples show magnetic signal, probably due to the existence of magnetically active Co atoms randomly distributed in the amorphous network. For the annealed samples, due to the diffusion of Co and the structural rearrangement of the network, it is expected that the number of magnetically active Co atoms increase (Ko et al., 2006). However, its magnetic activity does not exceed that of the amorphous films due to the formation of $CoGe_2$. Finally, the increasing in the magnetic signal with increasing [Co] is expected since the number of magnetically active Co atoms probably also increases.

For the SiCo films, the situation seems somewhat different, and not systematic. At first, as shown in Fig. 12(a), the sample with [Co] ~ 2.8 at.% without annealing shows a relatively high value of magnetic signal due to the magnetically active Co. After annealing at 900 $^{\circ}$C, its value is diminished, probably due to the formation of $CoSi_2$. In contrast, the as-deposited Si film with the highest [Co] (~ 10.3 at.%) presents an extremely low MFM signal, probably due to the large number of magnetically inactive Co atoms, which may be associated with its highly disordered structure. After annealing at 900 $^{\circ}$C, its magnetic activity is significantly increased due to the diffusion and consequent magnetic activation of the Co atoms. However, the magnetic activity is now limited by the existence of $CoSi_2$, and, therefore, its magnetism is less intense than the as-deposited film with [Co] ~ 2.8 at.%, that, in principle, doesn't have the silicide phase.

7. Conclusion

In summary, MFM is a relatively new technique for imaging magnetization patterns with high resolution and minimal sample preparation. The technique is an offspring of AFM and employs a sharp magnetic tip attached to a flexible cantilever. The tip is placed close to the sample surface (from some nanometres to a few micrometres) and interacts with the stray field emanating from the sample. The image is formed by scanning the tip laterally with respect to the sample and measuring the force (or force gradient) as a function of position. The interaction strength is then determined by monitoring the motion of the cantilever using a sensor. Although a lot of effort has been done in order to get quantitative information, MFM is still predominantly a qualitative characterization technique. In the present work, MFM proved to be particularly suitable to study the magnetic properties of Si and Ge-based magnetic semiconductors. In this context, the technique is very efficient to detect magnetic activity in the form of vortices in sub-micrometre structures. As well, a combination of the

MFM and SQUID techniques can be very convenient to probe the magnetic properties of microsized (or sub-microsized) isolated structures.

8. Acknowledgments

9. References

Affouda C. A., Bolduc M., Huang M. B., Ramos F., Dunn K. A., Thiel B., Agnello G., & LaBella V. P. (2006). Observation of crystallite formation in ferromagnetic Mn-implanted Si, *The Journal of Vacuum Science and Technology A,* Vol. 24, No. 4, pp. 1644-1647.

Bernardini F., Picozzi S., & Continenza A. (2004). Energetic stability and magnetic properties of Mn dimers in silicon, *Applied Physics Letters,* Vol. 84, No. 13, pp. 2289-2291.

Bolduc M., Affouda C. A., Stollenwerk A., Huang M. B., Ramos F. G., Agnello G., & Labella V. P. (2005). Above room temperature ferromagnetism in Mn-ion implanted Si, *Physical Review B,* Vol. 71, No. 3, pp. 033302-1−033302-4.

Bruker Corporation. (2011). MESP tips, In: *Bruker AFM Probes*, 23.09.2011, Available from: http://www.brukerafmprobes.com/Product.aspx?ProductID=3309.

Cho S., Choi S., Hong S. C., Kim Y., Ketterson J., Kim B. J., Kim Y. C., & Hung J. H. (2002). Ferromagnetism in Mn-doped Ge, *Physical Review B,* Vol. 66, No. 3, pp. 033303-1−033303-3.

Continenza A., Profeta G., & Picozzi S. (2006). Transition metal impurities in Ge: chemical trends and codoping studied by electronic structure calculations, *Physical Review B,* Vol. 73, No. 3, pp. 035212-1−035212-10.

Dietl T. & Ohno H. (2006). Engineering magnetism in semiconductors, *Materials Today,* Vol. 9, No. 11, pp. 18-26.

Ferri F. A. & Zanatta A. R. (2009). Structural, optical and morphological characterization of amorphous $Ge_{100-x}Mn_x$ films deposited by sputtering, *Journal of Physics D: Applied Physics,* Vol. 42, No. 3, pp. 035005-1−035005-6.

Ferri F. A. (2010). *Synthesis and characterization of Si and Ge based films doped with magnetic species*, PhD Thesis, Instituto de Física de São Carlos, Universidade de São Paulo, São Carlos, Brazil.

Ferri F. A., Pereira-da-Silva M. A., & Zanatta A. R. (2009). Evidence of magnetic vortices formation in Mn-based sub-micrometre structures embedded in Si–Mn films, *Journal of Physics D: Applied Physics,* Vol. 42, No. 13, pp. 132002-1−132002-5.

Ferri F. A., Pereira-da-Silva M. A., & Zanatta A. R. (2011). Development of the $MnSi_{1.7}$ phase in Mn-containing Si films, *Materials Chemistry and Physics,* Vol. 129, No. 1-2, pp. 148-153.

Ferri F. A., Pereira-da-Silva M. A., Zanatta A. R., Varella A. L. S., & de Oliveira A. J. A. (2010). Effect of Mn concentration and atomic structure on the magnetic properties of Ge thin films, *Journal of Applied Physics,* Vol. 108, No. 11, pp. 113922-1−113922-5.

Hartmann U. (1999). Magnetic force microscopy, *Annual Review of Materials Research,* Vol. 29, pp. 53-87.

Hendrych A., Kubínek R., & Zhukov A. V. (2007). The magnetic force microscopy and its capability for nanomagnetic studies - The short compendium, In: *Modern Research and Educational Topics in Microscopy*, Méndez-Vilas A. & Díaz J., (Eds.), Vol. 2, pp. 805-811, Formatex, ISBN 13: 978-84-611-9420-9, Badajoz, Spain.

Kim S. K., Cho Y. C., Jeong S. Y., Cho C. R., Park S. E., Lee J. H., Kim J. P., Kim Y. C., & Choi H. W. (2007). High-temperature ferromagnetism in amorphous semiconductor Ge_3Mn thin films, *Applied Physics Letters,* Vol. 90, No. 19, pp. 192505-1−192505-3.

Ko V., Teo K. L., Liew T., & Chong T. C. (2006). Ferromagnetism and anomalous Hall effect in $Co_xGe_{1−x}$, *Applied Physics Letters,* Vol. 89, No. 4, pp. 042504-1−042504-3.

Koch S. A. (2005). *Functionality and dynamics of deposited metal nanoclusters*, PhD Thesis, Groningen University Press, ISBN 90-367-2289-6, Groningen, The Netherlands.

Martin Y. & Wickramasinghe H. K. (1987). Magnetic imaging by "force microscopy" with 1000 $\overset{o}{A}$ resolution, *Applied Physics Letters*, Vol. 50, No. 20, pp. 1455-1457.

Porthun S., Abelmann L., & Lodder C. (1998). Magnetic force microscopy of thin film media for high density magnetic recording, *Journal of Magnetism and Magnetic Materials,* Vol. 182, No. 1-2, pp. 238-273.

Rasa M., Kuipers B. W. M., & Philipse A. P. (2002). Atomic force microscopy and magnetic force microscopy study of model colloids, *Journal of Colloid and Interface Science,* Vol. 250, No. 2, pp. 303-315.

Rugar D., Mamin H. J., Guethner P., Lambert S. E., Stern J. E., McFadyen I., & Yogi T. (1990). Magnetic force microscopy: General principles and application to longitudinal recording media, *Journal of Applied Physics*, Vol. 68, No. 3, pp. 11694-1184.

Schwarz A. & Wiesendanger R. (2008). Magnetic sensitive force microscopy, *Nanotoday*, Vol. 3, No. 1-2, pp. 28-39.

Shinjo T., Okuno T., Hassdorf R., Shigeto K., & Ono T. (2000). Magnetic vortex core observation in circular dots of permalloy, *Science,* Vol. 289, No. 5481, pp. 930-932.

Soares M. M., Biasi E., Coelho L. N., Santos M. C., Menezes F. S., Knobel M., Sampaio L. C., & Garcia F. (2008). Magnetic vortices in tridimensional nanomagnetic caps observed using transmission electron microscopy and magnetic force microscopy, *Physical Review B,* Vol. 77, No. 22, pp. 224405-1−224405-7.

Zhang F. M., Liu X. C., Gao J., Wu X. S., Du Y. W., Zhu H., Xiao J. Q., & Chen P. (2004). Investigation on the magnetic and electrical properties of crystalline $Mn_{0.05}Si_{0.95}$ films, *Applied Physics Letters,* Vol. 85, No. 5, pp. 786-788.

Zhu X., Grütter P., Metlushko V., & Ilic B. (2002). Magnetization reversal and configurational anisotropy of dense permalloy dot arrays, *Applied Physics Letters,* Vol. 80, No. 25, pp. 4789-4791.

Zutic I., Fabian J., & DasSarma S. (2004). Spintronics: Fundamentals and applications, *Reviews of Modern Physics,* Vol. 76, No. 2, pp. 323-410.
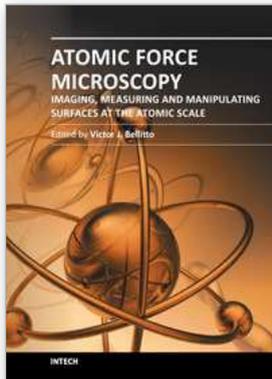
Atomic Force Microscopy - Imaging, Measuring and Manipulating Surfaces at the Atomic Scale
Edited by Dr. Victor Bellitto

With the advent of the atomic force microscope (AFM) came an extremely valuable analytical resource and technique useful for the qualitative and quantitative surface analysis with sub-nanometer resolution. In addition, samples studied with an AFM do not require any special pretreatments that may alter or damage the sample and permits a three dimensional investigation of the surface. This book presents a collection of current research from scientists throughout the world that employ atomic force microscopy in their investigations. The technique has become widely accepted and used in obtaining valuable data in a wide variety of fields. It is impressive to see how, in a short time period since its development in 1986, it has proliferated and found many uses throughout manufacturing, research and development.

How to reference
In order to correctly reference this scholarly work, feel free to copy and paste the following:

F.A. Ferri, M.A. Pereira-da-Silva and E. Marega Jr. (2012). Magnetic Force Microscopy: Basic Principles and Applications, Atomic Force Microscopy - Imaging, Measuring and Manipulating Surfaces at the Atomic Scale, Dr. Victor Bellitto (Ed.), ISBN: 978-953-51-0414-8, InTech, Available from:
http://www.intechopen.com/books/atomic-force-microscopy-imaging-measuring-and-manipulating-surfaces-at-the-atomic-scale/magnetic-force-microscopy-basic-principles-and-applications

INTECH
open science | open minds